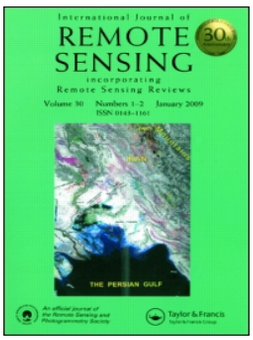

International Journal of Remote Sensing

ISSN: 0143-1161 (Print) 1366-5901 (Online) Journal homepage: http://www.tandfonline.com/loi/tres20

Object-based road extraction from satellite images using ant colony optimization

Mehdi Maboudi, Jalal Amini, Michael Hahn & Mehdi Saati

To cite this article: Mehdi Maboudi, Jalal Amini, Michael Hahn & Mehdi Saati (2017) Object-based road extraction from satellite images using ant colony optimization, International Journal of Remote Sensing, 38:1, 179-198, DOI: 10.1080/01431161.2016.1264026

To link to this article: http://dx.doi.org/10.1080/01431161.2016.1264026

Published online: 12 Dec 2016.

INTERNATIONAL JOURNAL OF REMOTE SENSING, 2017
VOL. 38, NO. 1, 179–198
http://dx.doi.org/10.1080/01431161.2016.1264026

Taylor & Francis
Taylor & Francis Group

Object-based road extraction from satellite images using ant colony optimization

Mehdi Maboudi [a,b], Jalal Amini[a], Michael Hahn[b] and Mehdi Saati[a]

[a]School of Surveying and Geospatial Engineering, College of Engineering, University of Tehran, Tehran, Iran; [b]Faculty of Geomatics, Computer Science and Mathematics, University of Applied Sciences, Stuttgart, Germany

ABSTRACT

Increasing demands for up-to-date road network and the availability of very-high-resolution (VHR) satellite images as well as the popularity of high-speed computers provide motivation and preliminary materials for researchers to propose more advanced approaches in order to increase the automation and robustness of road extraction strategies. In this article, road characteristics are modelled via object-based image analysis (OBIA). Object-based information is embedded as heuristic information in the ant colony optimization (ACO) algorithm for handling the road network extraction problem. A new neighbourhood definition in object space is introduced, which affects the transition rule in order to decrease the road gaps. Furthermore, an innovative desirability function for ACO is designed, which extracts the road objects, competently. The experimental results demonstrate the efficiency of the proposed algorithm for road extraction from VHR images. Moreover, the results of two state-of-the-art methods are compared with the proposed algorithm.

ARTICLE HISTORY
Received 20 July 2016
Accepted 13 November 2016

1. Introduction

The different aspects of daily life of most people and the prosperity of many communities are inextricably intertwined with the roads. Therefore, the demand for accurate and up-to-date roadmaps is high. In light of the variety of applications, roads are of special importance among various man-made objects (Z. Li et al. 2015; Ameri and ValadanZoej 2015; Saati, Amini, and Maboudi 2015). These applications that support human civilization in different ways include, but are not restricted to, emergency services, urban design, navigation, transportation applications, and post-hazard rescue (Samadzadegan and Zarrinpanjeh 2008; Das, Mirnalinee, and Varghese 2011; Ravanbakhsh, Heipke, and Pakzad 2008).

The ability of advanced Earth observation satellite imaging sensors, such as IKONOS, QuickBird, GeoEye, and WorldView series, to deliver very-high-resolution (VHR) images opens a new era for the remote sensing and digital mapping of the Earth's surface and calls for the development of automatic tools to decrease human inference in urban

CONTACT Mehdi Maboudi mmaboudi@ut.ac.ir School of Surveying and Geospatial Engineering, College of Engineering, University of Tehran, Tehran, Iran

feature extraction and identification (Rahimi, Arefi, and Bahmanyar 2015; Mokhtarzade and ValadanZoej 2007). As a by-product of this significant improvement in spatial resolution, the amount of data to be processed and the spatial details that should be managed increase. Therefore, alternative paths have been followed by remote-sensing and computer science researchers in order to derive meaningful objects that are made up of several pixels. Object-based image analysis (OBIA), also known as geospatial object-based image analysis (GEOBIA), is introduced as a promising solution for such problems in the pixel-based processing of VHR satellite images (Blaschke 2010). Considering objects as the lowest level of processing entities in VHR images leads to better feature space separation, which is mainly caused by efficiently employing the shape features and mutual relations between image objects. Moreover, image objects can be related to real objects, more closely (Benz et al. 2004). Therefore, the mainstream OBIA is of particular interest for road extraction from VHR images (Maboudi, Amini, and Hahn 2016; Miao et al. 2015).

A rich body of literature exists in road extraction from different types of remotely sensed data. Some articles have studied many of these approaches (Mena 2003; Y. Li, Xu, and Piao 2009; Das, Mirnalinee, and Varghese 2011; Quackenbush, Im, and Zuo 2013; W. Wang et al. 2016; Maboudi et al. 2016). In this article, we just mention some distinguished articles that are decidedly related to the scope of our research.

In Grote, Heipke, and Rottensteiner (2012), a region-based approach is proposed, which divides the image into some tiles and then over-segments them by a graph-cut segmentation. Then the regions are grouped to construct meaningful objects. Finally, a fuzzy rule-based classification separates road regions from other regions.

An object-based method for road network extraction in VHR satellite images has been proposed by Miao et al. (2015). In their approach, an Iterative Self-Organizing Data Analysis Technique algorithm (ISODATA) divides the image pixels into objects. Next, a Support Vector Machine (SVM) is exploited to extract the road objects.

In Nikfar et al. (2015), an object-based road extraction method is proposed, which segments the IKONOS images using multi-resolution segmentation. Then, a type-II fuzzy logic system is adopted to select the optimum classification rules for the detection of road objects.

The multi-resolution segmentation, implemented in eCognition software, is employed by M. Li et al. (2016) to generate the initial regions. After removing vegetation, shadow, and buildings, a region-merging method based on binary partition tree (BPT), followed by two fuzzy rules, is adopted to detect the road regions.

An ant-based roadmap updating framework is proposed in Zarrinpanjeh, Samadzadegan, and Schenk (2013). In their distributed framework, the authors verify an existing roadmap and then start a search for new roads. Finally, the results are grouped to achieve the final road network.

More recently, in Yin et al. (2015) segmentation is performed by a mean-shift algorithm to achieve the basic edge and polygon information. The authors postulate the consistency of the direction for the most objects in the road contexts. Based on this idea, an ant colony optimization (ACO) is extended to extract the main roads from QuickBird images.

Most recent algorithms use object (region)-based strategies for road extraction from VHR imageries. The initial inspiration and motivation for our research come from the fact

that object-based image information can be formulated and utilized as heuristic information in ACO to leverage the suitability of ACO in handling the network-related problems for the automatic extraction of road network from VHR images. Therefore, in this article, a new approach based on OBIA and ACO is proposed for the road extraction problem. Object-based descriptors are embedded in ACO (as a swarm intelligence algorithm) in order to extract the road network from VHR remotely sensed data. The main difference between the proposed approach and the two preceding ant-based road extraction approaches, that is, Zarrinpanjeh, Samadzadegan, and Schenk (2013) and Yin et al. (2015), is that the former generally presents a framework for updating an existing road network and the latter mainly rely on edge information of the image to extract the main roads. However, in our approach, no ancillary data, such as vector data provided by road databases, is employed and it generally takes advantage of object-based descriptors of the roads segments. Additionally, a novel heuristic function, which simultaneously employs structural and spectral characteristics of the road in ACO, is presented. Furthermore, a new neighbourhood definition in object space is introduced, which affects the transition rule of ACO in order to decrease the road gaps.

The remainder of this article is organized as follows. Section 2 describes the general aspects of the proposed approach. Image segmentation, object-based descriptors, and the basic principles of the ACO as well as our problem-dependent customization of ACO are also presented in Section 2. The experimental results are reported in Section 3, and finally, the closing discussion and conclusion are presented in Section 4.

2. Methodology

The overview of the proposed object-based approach for road network extraction from satellite images using ACO is depicted in Figure 1.

As can be seen from Figure 1, the VHR image is segmented using multi-resolution segmentation in order to generate image objects. Considering the characteristics of roads in the image, structural and spectral descriptors are computed for each object. These descriptors can be considered as a feature vector for objects to enter the ACO.

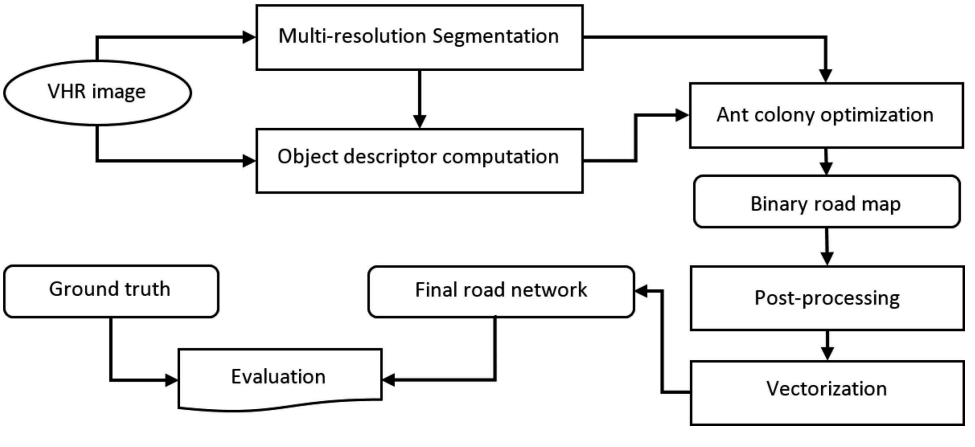

Figure 1. Overview of the proposed approach.

Considering objects as nodes of a graph, ant agents move through the object space graph and try to connect the nodes to generate a binary roadmap. Later, a post-processing step is utilized to improve the quality of the extracted roadmap. Finally, the binary roadmap is vectorized to achieve the centrelines of the road network. To evaluate the performance of the approach, the extracted road network is compared with the ground truth data utilizing three geometric evaluation criteria, including completeness, correctness, and quality.

2.1. *Segmentation*

Image segmentation is a fundamental yet challenging aspect of OBIA and its quality has a significant influence on succeeding operations (Grote, Heipke, and Rottensteiner 2012; Maboudi and Amini 2015). This step is crucial since it provides the basic entities on which later processes will be applied (Tabib Mahmoudi, Samadzadegan, and Reinartz 2013). Several approaches are presented in the literature for the segmentation of remotely sensed images. The state-of-the-art image segmentation algorithms for remote-sensing images can be classified into four general categories (Schiewe 2002; M. Wang and Li 2014): 1) pixel (threshold-based) methods; 2) region-based methods; 3) edge-based methods; and 4) hybrid approaches. In this article, the multi-resolution segmentation, formerly known as the fractal net evolution approach (FNEA), introduced in Baatz and Schäpe (2000), is utilized for image segmentation. Multi-resolution segmentation is a well-recognized region-based approach that exploits both spectral and shape properties to decrease the heterogeneity of the segments. Initially, this approach considers each pixel of the image as an object. Next, during an iterative procedure, according to a fusion factor, a pair of objects merges into a larger object. The fusion factor, which represents the cost of fitting, can be formulated as follows (Saba, ValadanZoej, and Mokhtarzade 2016):

$$f = W_{\text{color}} h_{\text{color}} + W_{\text{shape}} h_{\text{shape}}, \tag{1}$$

where W_{color} and W_{shape} are the weight of spectral (colour) heterogeneity and the weight of shape heterogeneity, respectively; h_{color} and h_{shape} are the difference in the spectral heterogeneity and difference in the shape heterogeneity, respectively; and $W_{\text{color}} + W_{\text{shape}} = 1$. The difference in spectral heterogeneity between two objects in a multispectral image with B bands is defined as follows:

$$h_{\text{color}} = \sum_{b=1}^{B} W_b \left\{ n_{\text{m}} \sigma_{b,\text{m}} - \left(n_1 \sigma_{b,1} + n_2 \sigma_{b,2} \right) \right\}, \tag{2}$$

where W_b is the weight of each band and the indices 1, 2, and m represent the first, second, and merged objects, respectively. n is the number of pixels in each object and σ shows the standard deviation of the spectral values of pixels that form the object. The difference in shape heterogeneity between two objects consists of two factors, called smoothness and compactness heterogeneities. Considering W_{smooth} and W_{comp} as the weight of the smoothness and compactness heterogeneities, respectively, the difference in shape heterogeneity is defined as follows:

$$h_{\text{shape}} = W_{\text{smooth}}\left\{n_{\text{m}}\frac{\ell_{\text{m}}}{p_{\text{m}}} - \left(n_1\frac{\ell_1}{p_1} + n_2\frac{\ell_2}{p_2}\right)\right\} + W_{\text{comp}}\{\ell_{\text{m}}\sqrt{n_{\text{m}}} - (\ell_1\sqrt{n_1} + \ell_2\sqrt{n_2})\}, \quad (3)$$

where ℓ is the factual length of the object, p is the perimeter of the minimum bounding box of the object, and $W_{\text{smooth}} + W_{\text{comp}} = 1$.

2.2. *Swarm intelligence and ACO*

Bio-inspired swarm intelligence has attracted great interest in the last two decades (Yang et al. 2013). These algorithms include, but are not limited to, Particle Swarm Optimization (PSO), ACO, Artificial Bee Colony (ABC), Firefly algorithm, Bat algorithm, and Cuckoo search (CS). These swarm-based algorithms try to roughly imitate the behaviour of the real population of creatures in solving some problems that their deterministic solutions (if exist) are not optimal in some interested aspects (Yang et al. 2013). Real-world intelligent societies, which may show a simple intelligence individually, can solve sophisticated problems that are beyond the capabilities of each individual (Dorigo, Bonabeau, and Theraulaz 2000). Among all these approaches, ACO exhibited very good performance in discrete and network-based problems. Furthermore, the applicability of the parallel processing of ACO and the promising results of the implementation of ACO metaheuristic on graphics processing units (GPUs) (Delévacq et al. 2013) pave the way for implementing fast and efficient object detection algorithms based on ACO.

The remainder of this section sketches out the general procedure of the ACO. Then, fundamental parts of the ACO algorithm in our implementation are described in detail. It needs to be accentuated that many ant colony algorithms exist in the literature, which try to imitate the behaviour of real forager ants. Most of them are similar in principles, as mentioned in the next paragraph, and some differences in the imitation of different steps separate them from each other.

To start with, the ant colony algorithm selects n segments and places an ant on each segment ('breeding'). The initial pheromone value on each edge is set to a very small amount $\tau_0 > 0$. Then each ant starts searching the environment. It examines the neighbours ($\mathcal{N}$) to find high-quality connections. The ant gives a score or probability of selection to each edge and selects its next destination by analysing their descriptors vector **F** and pheromone of the edge. In most cases, it selects one of the high-quality edges based on their associated probability ('transition rule'). The ant continues the journey and in each node makes a new selection. To avoid loops and to help the ant to explore its environment, a tabu list is assigned to each ant in order to ignore the recently visited edges. The ant continues the journey to meet a 'stopping criterion'. Here, the most important part of the mission is accomplished and the ant should go back to the nest. The final task is to mark the path in order to share its experiments with possible next colony members that traverse the same edge ('pheromone updating'). The other ants mostly follow the same rules as described above. The main difference is that the next colony members receive the former ants' cues, mediated by the environment, to tune their decision and find the high-quality paths more efficiently. The pseudo code of the proposed ACO can be considered as follows.

Initialization of the parameters.

for each edge (i,j) **do**

$\tau_{i,j} = \tau_0$

end

for each iteration **do**

Roulette wheel based breeding using SOLI index

for each ant $k \in \{1, 2, \ldots n\}$ at current node i **do**

$\text{path}_k = \emptyset$;

repeat

Define $\mathcal{N}_i^k$ (Section 2.2.2)

Select the next destination J according to Equations (4)–(5)

$\text{path}_k = \text{path}_k \cup (i, J)$

$i = J$

until at least one of the stopping criteria is fulfilled (Section 2.2.6)

end

pheromone updating (Section 2.2.4)

end

2.2.1. *Breeding*

A number of n ants are bred and keep moving in the graph until each of them reaches a stopping criterion. The easiest solution for selecting the initial points can be the random selection of n objects. However, in some studies, the ants are distributed based on problem-dependent information. For example, in Davoodianidaliki, Abedini, and Shankayi (2013), gradient magnitude image is used to select the start point of the ants for edge detection. In this research, we utilize *a priori* knowledge to guide the colony members to achieve better results. Therefore, we select n objects by constructing a roulette wheel (Floreano and Mattiussi 2008), in which the size of its slots corresponds to the elongation of the objects measured by the skeleton-based object linearity index (SOLI) (Maboudi et al. 2016). According to the roulette wheel selection definition, the probability that an object is selected is given by the ratio between its SOLI value and the sum of the SOLI values of all objects in the scene. Thus, the elongated objects have more chance to be selected as initial points, which improves the convergence of the algorithm.

2.2.2. *Object-based neighbourhood definition*

Unlike most ACO implementations, such as that of Yin et al. (2015), which defines the same fixed vision radius in 2D Euclidean space for all ants, in our approach, the visible area for each ant is defined in object space. Moreover, we expand the vision radius (r) in object space to $r = 2$, which means that each ant on a node can see the instant neighbours of that node, as well as their neighbours. Therefore, the Euclidean vision area for each ant can be completely different from others' in 2D Euclidean space. This new neighbourhood affects the transition rule in Equation (5), and enables the ants to get rid of the most possible occlusions and over-segmented regions. In standard ACO, the heuristic information of each edge (i,j) is used to add the problem-dependent desirability of that edge to

the decision-making process. However, using the proposed object-based neighbourhood definition, all ants consider their neighbouring edges as well as the best neighbour of those neighbours (Equation (7)) in order to select their next destination. Thus, in case of a gap or over-segmentation, according to Equation (6), the desirable neighbour of a neighbour may be selected, which leads to efficient gap filling.

2.2.3. *Transition rule*

In the symmetric travelling salesman problem (TSP) problem, the distance between each pair of nodes is considered as the cost of travel and all the nodes are alike. Thus, an undirected graph can be used in the implementation. However, in the object-based road detection, some descriptors are mutual, that is, are related to both nodes of an edge, such as spectral similarity, and each node also has its own characteristics, such as shape of the segment. Figure 2(*a*,*b*) show this difference schematically.

In Figure 2(*a*), the graph of a simple TSP is depicted. In Figure 2(*b*), the size of each node shows the desirability of that node. To address this problem-dependent situation, we define a directed graph, instead of an undirected graph, in case of the symmetric TSP problem. A directed graph, which is conceptually similar to the graph used in our approach, is shown in Figure 2(*c*). It means the desirability between two nodes may be different due to the difference between their characteristics. The length of the directed edges between each pair of nodes are inversely related to their relative desirability. Thus, in Figure 2(*c*), the distance from a node to another smaller (less desirable) node, which is drawn in red, is longer than the inverse path, which is drawn in blue.

This graph configuration affects the similarity of the adjacency matrix and leads to a pseudo-symmetric adjacency matrix.

A combination of random selection, proportional selection, and greedy selection is used to select the next destination. Before each movement, a random number is generated and the next destination is selected using an equation as follows:

$$J = \begin{cases} \text{random proportional} & \geq q_0 \in [01] \\ \text{greedy selection} & \text{otherwise} \end{cases}, \tag{4}$$

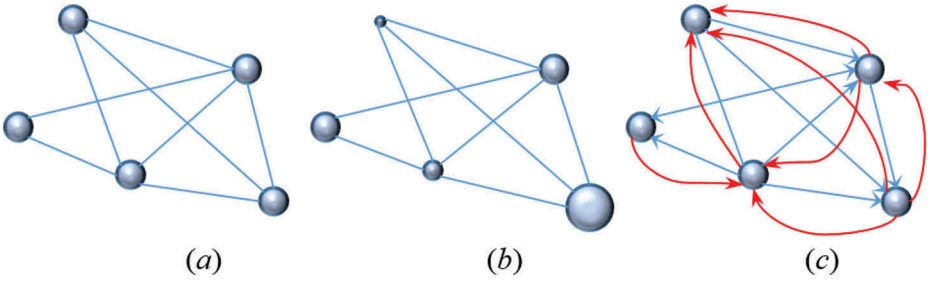

Figure 2. Schematic graph representation of a symmetric TSP and our approach's graph. (*a*) TSP graph; (*b*) our approach's graph (differences in node properties are shown by their size); (*c*) directed graph (differences in nodes are considered as different edges between two nodes. Red arrows show longer distances, that is, higher transition costs, and blue arrows show shorter distances, i.e. lower transition cost) .

where q_0 is a parameter that balances the intensification and diversification abilities of the algorithm. For random selection, a roulette wheel selection algorithm is used. The ant (k) located on a node (i) at the state (t) selects the next destination (J) randomly, by using all valid neighbours $\left(\mathcal{N}_i^k\right)$ as prescribed alphabets (roulette wheel slots). The probability of selecting each edge of the graph in Figure 2(*c*) is related to the size of the corresponding roulette wheel slot and is computed as follows:

$$p_{ij}(t) = \frac{\tau_{ij}(t)\gamma_{ij}^{\beta}}{\sum_{j\in\mathcal{N}_i^k}\tau_{ij}(t)\gamma_{ij}^{\beta}} \qquad \forall j \in \mathcal{N}_i^k \tag{5}$$

where τ is the pheromone concentration of each edge, which is initially set to τ_0, β is a positive value used to amplify the influence of attractiveness (or potential benefit) of moves, and γ is the modified desirability of each edge, which is formulated as follows:

$$\gamma_{ij} = \max\left(\eta_j^*, \eta_{ij}\right), \tag{6}$$

where η_{ij} is the desirability of the edge between i and j and η_j^* is the heuristic information of the most desirable neighbouring edge of j, which is defined as

$$\eta_j^* = \max_{\forall u\in\mathcal{N}_j^k}\left(\eta_{ju}\right). \tag{7}$$

For greedy selection, instead of pseudo-random proportional selection of the next node, just the node with the maximum probability of selection is selected as J. Here, the normalization of the probabilities is not necessary any more.

2.2.4. *Pheromone updating*

Forager ants primarily use pheromone to communicate with their colony members (nest-mates). Despite some other social insects, where each member communicates with other individuals of the colony directly, such as waggle dance of a honeybee (Saeedi, Samadzadegan, and El-Sheimy. 2009), the communication between foraging ants is indirect. These ants lay an amount of pheromone on the trail and by this means change the environment, which may affect the behaviour of the nest-mates who will arrive in this modified environment in the future. This specific type of indirect communication between ants is called *stigmergy*.

In each iteration, since all n ants have made their solutions, a pheromone-updating procedure is undertaken. This step consists of two parts, namely pheromone evaporation and pheromone intensification, which is formulated as follows (Dorigo, Bonabeau, and Theraulaz 2000):

$$\tau_{ij}(t+1) = \underbrace{(1-\rho)\tau_{ij}(t)}_{\text{evaporation}} + \underbrace{\Delta\tau_{ij}(t)}_{\text{intensification}}, \tag{8}$$

where $\rho \in [01]$ is the evaporation rate and denotes how much of the pheromone is diminished after each state.

The intensification part of Equation (8) is sum of the pheromones released by all ants that traversed this link recently:

$$\Delta\tau_{ij}(t) = \sum_{m}^{k=1} \Delta\tau_{ij}^{k}, \tag{9}$$

where m is the number of ants that passed this link at state t. The amount of pheromone that each ant releases on an edge is a function of its solution quality and can be defined as follows:

$$\Delta\tau_{ij}^{k}(t) = \sum_{\forall E \in S} w_b \eta_{\mathrm{E}}, \tag{10}$$

where b is the node index, η_{E} is desirability of the edge, and w is the importance of the object, which is defined as its area.

2.2.5. *Heuristic information*

The heuristic information is a problem-dependent value, which adds an explicit bias towards the most desirable paths (Engelbrecht 2007). In the proposed approach for the road extraction problem, the heuristic information such as elongation and low spectral heterogeneity are defined via descriptors of the objects to make the road-like segments more desirable for artificial ant agents.

Road object descriptors. The structural, spectral, and topological properties of a road enable humans to recognize it in an image (Mirnalinee, Das, and Varghese 2011). Elongation and width uniformity are the main structural characteristics of the road, which, with the support of low spectral heterogeneity, can be used to distinguish road segments from background.

Considering the rectangularity aspect of road segments, the SOLI is embedded in the transition rule of ACO as heuristic information. The SOLI is defined for each object as follows:

$$\mathrm{SOLI}_{\mathrm{obj}} = \begin{cases} \frac{L_s^2}{n_{\mathrm{obj}}} & \text{if } D_{\mathrm{obj}} \in W_{\mathrm{R}} \\ 0 & \text{otherwise} \end{cases}, \tag{11}$$

where obj is an object index,n_{obj} is the number of pixels in the object, L_s is the length of the main line of the object's skeleton, W_{R} is the width range of roads appearing in the image, and D_{obj} is the maximum object-based distance map value of the object. Generally, for road segments, the value of this linearity index should be high. Therefore, segments with small values of SOLI should be weighted appropriately to have a low desirability for ant agents.

As mentioned before, road segments tend to have low spectral standard deviation. Furthermore, the length of the road segments is usually high. Therefore, these characteristics should be applied in the heuristic function of the ACO in such a way that high standard deviation of grey values and low length of an object result in decreasing desirability of that object. Furthermore, some misleading situations should be avoided, for example, a very homogenous bright building roof near a homogenous but dark road segment. In this case, both regions may have low standard deviation, but the ants that are

located on the road surface should avoid selecting the building segments as their next destination. To address this problem, instead of spectral standard deviation we adopt the idea of difference in spectral heterogeneity (cf. Equation (2)) and define the spectral heterogeneity of object i and object j in the bth band of the VHR image as follows:

$$\xi_{i,j}^{b} = \left\{ n_{\mathrm{m}} \sigma_{b,\mathrm{m}} - \left(n_i \sigma_{b,i} + n_j \sigma_{b,j} \right) \right\}. \tag{12}$$

We should also take the size of the objects into account. Because in our application, that is, road detection, elongated objects are our focus, the spectral heterogeneity is weighted by the length of the merged object. Finally, the heuristic information of each edge is defined as

$$\eta_{i,j} = (\mathrm{SOLI})_j e^{-\left(\prod_{B}^{b=1} \xi_{i,j}^{b} \frac{}{L} \right)^2} \mathcal{H}_T(\mathrm{NDVI})_j, \tag{13}$$

where i and j are the indices of the nodes constructing the graph edge,L is the length of the merged object, B is the cardinality of the VHR image bands set, $\mathcal{H}$ is the Heaviside step function of NDVI, and T is a parameter for controlling the shape of $\mathcal{H}$. All other notations are in accordance with those mentioned before.

2.2.6. *Stopping criteria*

In our ACO implementation, each ant finishes its journey through the graph whenever at least one of the following criteria is fulfilled: (1) the ant reaches a previously traversed edge; (2) the ant arrives at the boundary of the image; (3) the best neighbouring node of the current location of the ant is not desirable enough to be a road segment; (4) the ant cannot find an unvisited neighbouring node. Since an ant reaches a stopping criterion, at the end of the current state, it goes back to the nest in the opposite way of its journey and intensifies the amount of pheromone during its return trip according to Equation (10).

2.3. *Post-processing and vectorization*

The quality of the detected roadmap can be improved by applying some refinement. First, a region part segmentation algorithm (Bennamoun and Mamic 2002; Das, Mirnalinee, and Varghese 2011) is used to supress the incorrectly detected blobs that are attached to the binary roadmap. After this step, to convert the result of the road detection process to a vector map, the morphological thinning approach followed by the Douglas–Peucker algorithm (Shi and Cheung 2006) is employed. The final problem that should be solved is that due to many occlusions and obstacles, the achieved road centreline is not smooth enough. To address this problem, the *B*-spline model is used. In this step, the extracted road centreline points after the branch removal step are regarded as the initial control points for the *B*-spline model.

3. Experimental results

3.1. *Study area*

The efficacy and efficiency of the proposed swarm-based methodology are evaluated for automatic road extraction from the VHR satellite image. The first study area is located in Moonah, Australia. Moonah is a part of the city of Hobart, which is the capital city of the state of Tasmania, Australia. The targeted area, which covers 700 × 1300 m on the ground, has different types of road containing highly curved roads with different shapes, dead-ends, and culs-de-sac. Some trees cast shadow on some parts of the road network. Additionally, the existence of some driveways, round-abouts, and different forms of junctions in this area make the road network extraction more complicated. Figure 3(*a*) shows the location of the study area. The visible bands of the satellite image of the study area are depicted in Figure 3(*b*).

Four multispectral bands of IKONOS satellite images of these areas with 4 m spatial resolution as well as a panchromatic band with 1 m spatial resolution are used for this research. The data set is publicly available via the ISPRS website (ISPRS 2014). The Gram–Schmidt pan-sharpening method is employed to fuse the multispectral bands with the panchromatic band. The ground truth of this data set, which is delineated manually by an expert operator, is shown in Figure 3(*c*).

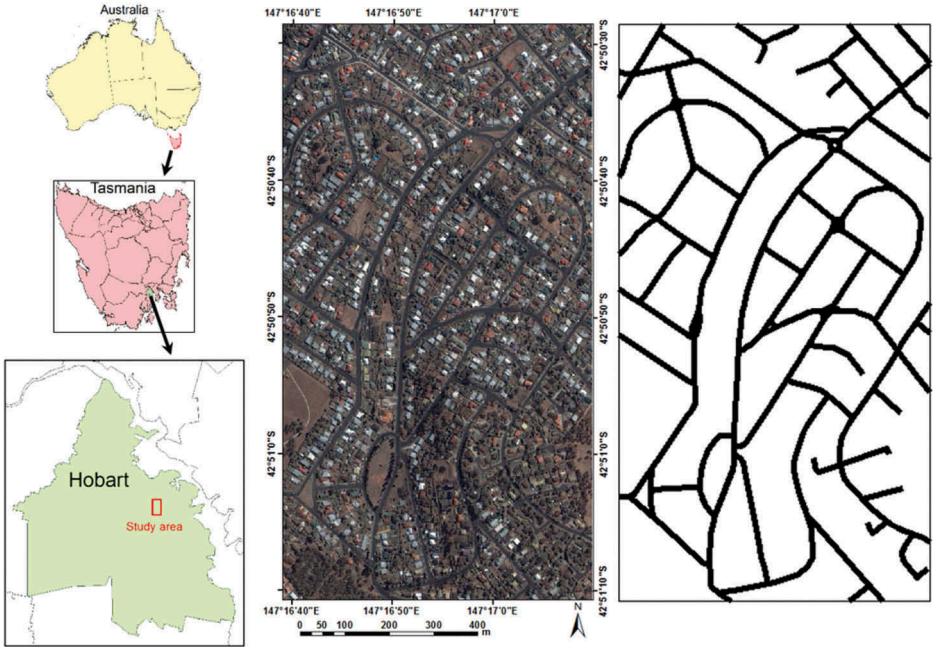

Figure 3. First study area. (*a*) The spatial location of the study area; (*b*) VHR satellite image of the study area; (*c*) ground truth.

3.2. *Evaluation criteria*

In our experiments, the qualitative assessment of the results is performed by using the three metrics defined in Wiedemann et al. (1998), which are used in most road extraction studies. To evaluate the results, the extracted road network is compared with ground truth and three values are computed as follows.

- True positive (TP): length of the correctly extracted road network;
- False negative (FN): length of the missing parts of the reference network in the extraction result; and
- False positive (FP): length of the wrongly extracted road network.

Based on these three values, three metrics are calculated as follows.

The first criterion shows the completeness of the results:

$$\text{Completeness} = \frac{(\text{TP})}{(\text{TP}) + (\text{FN})}. \tag{14}$$

The second criterion shows the correctness of the results:

$$\text{Correctness} = \frac{(\text{TP})}{(\text{TP}) + (\text{FP})}. \tag{15}$$

The third criterion is quality, which can be considered as follows:

$$\text{Quality} = \frac{(\text{TP})}{(\text{TP}) + (\text{FN}) + (\text{FP})}. \tag{16}$$

Quality is a combination of completeness and correctness of the results and shows the overall goodness of the results.

3.3. *Parameters study*

In the first step of this experiment, multi-resolution segmentation is performed to create the initial objects. We used the optimized parameters proposed in Nikfar et al. (2015) for this data set, that is, $s = 43$, $W_{\text{shape}} = 0.5$ and $W_{\text{comp}} = 0.3$. Next, the objects descriptors for all 4846 objects are calculated. In this step, we need a rough estimation of the width of the roads to calculate the SOLI index. The range of the width of the roads in this data set is about [7 15] pixels.

After generating objects (graph nodes) and calculating their descriptors, we apply our ACO-based approach (cf. Section 2) to the constructed graph. ACO involves a number of parameters, which their sensitivity and impact on the result need to be analysed. The main parameters include q_0, β and ρ. The optimal suggested value for q_0 is between 1 and 0.75 (Stützle et al. 2012). Selecting large values for this parameter quickly leads to search stagnation and some road segments may thus be ignored in the selection step. On the other hand, small values of q_0 hinder the convergence of the algorithm to the good results. Thus, we set the initial value for q_0 to 0.75. In each state, the algorithm increases the value of q_0, gradually. This strategy leads to an efficient exploration of the

road segments in the initial iterations. Moreover, in subsequent iterations, the colony members prefer the road-like objects that are selected in previous iterations.

By proper tuning of the parameter β in Equation (5), ACO can strike a balance between exploration and exploitation. Higher values of β emphasize the heuristic value in the ants' solution construction and lower values have the same effect on the pheromone values. Thus, we tested the different values for β in order to find a proper value for this parameter. For each value of β, we run the algorithm 10 times and computed the evaluation criteria. Figure 4 illustrates the average performance of the algorithm for different values of β.

Figure 4 illustrates the results of three evaluation criteria for different values of β. For very small values of β, the ACO algorithm mostly relies on ants' experiences, which are transferred by their pheromone and the heuristic information has less impact on the solution construction. Therefore, few parts of the network are detected correctly. How this shows up in the evaluation criteria can be easily found in the low completeness, correctness, and quality of the results. As β increases, the properties of the segments that are embedded in the heuristic part of Equation (5) play a more important role. Hence, these properties provide a higher probability of selection for road-like objects. This leads to an increase in the evaluation criteria. Large values of β decrease the completeness, because of the meta-heuristic characteristics of the ACO that diminish gradually. As a result, the desirability of edges would be too important for the ants in their decision-making process and they almost do not take advantage of other net-mates' experiences. Therefore, some parts of the network will not be discovered, which leads to an increase in the FN. In our experiments, ACO achieves the highest-quality results with β value around [2 3]. We set, $\beta = 2$ which provides the highest-quality result. This value will be used hereafter in our experiments.

The other parameter that should be investigated is evaporation rate (ρ), which is used in Equation (8). By using evaporation, the ACO avoids an unlimited increase of pheromone. Moreover, it helps the colony forget the previous poor constructions. Therefore, different values for ρ with the interval of 0.1 between its extremes, that is, [0 1], are selected. The result of our analysis on ρ is illustrated in Figure 5.

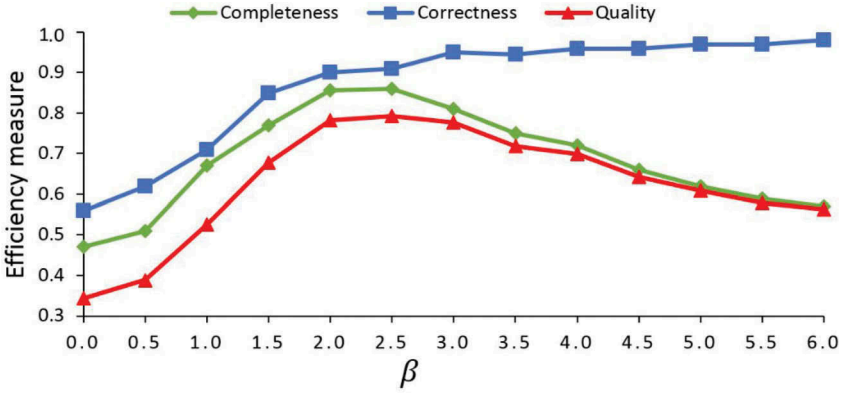

Figure 4. Performance curves for different β values.

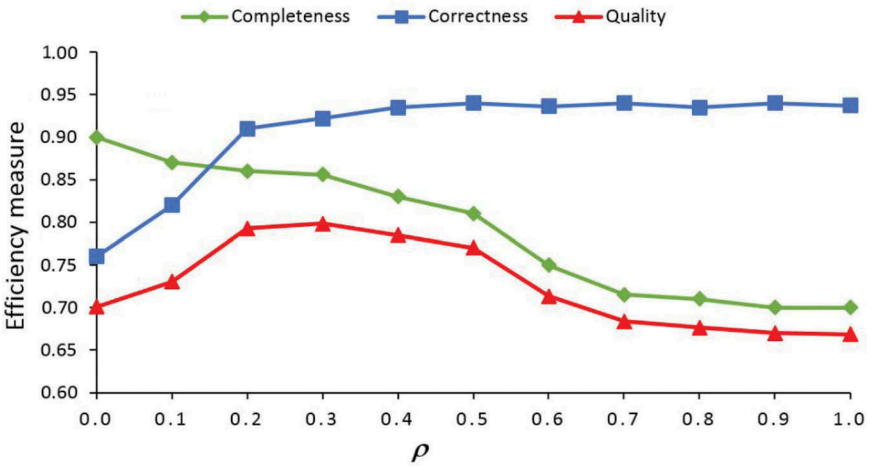

Figure 5. Performance curves for different ρ values.

Figure 5 compares the results of three evaluation criteria for different values of ρ. For very small values of ρ, that is, around zero, most parts of the road network are detected. However, this leads to a lower value of correctness. The reason is that without evaporation or at a very low evaporation rate, colony members do not forget the previously incorrect experiences and follow them again, which results in an increase in the amount of FPs. As ρ increases, the correctness increases; however, the algorithm also loses some correct, but not salient, detected road parts and hence the FN increases. Therefore, we must find a compromise between the correctness and completeness (i.e. the highest quality). In our experiments, ACO achieves the highest-quality result with a ρ value of around [0.2 0.4]. More exactly, we set, $\rho = 0.3$ and this value will be used through the following tests.

3.4. *First experiment result*

The randomly colour-coded results of the multi-resolution segmentation are depicted in Figure 6(*a*). The binary map produced by the above-mentioned selected values of the parameters is depicted in Figure 6(*b*). It can be seen from Figure 6(*b*) that the major problem in the result is some blobs that are attached to the road network. To address this problem, we use region part segmentation as mentioned in the post-processing step of the proposed approach in Section 2. Finally, thinning of the binary roadmap followed by the Douglas–Peucker algorithm (Shi and Cheung 2006) and *B*-spline interpolation is utilized to achieve the smooth centreline of the road network in vector format. For qualitative assessment, the result of road extraction by the proposed method is superimposed on the satellite image and is depicted in Figure 6(*c*).

It can be seen from Figure 6(*c*) that most parts of the network are extracted correctly. The proposed neighbourhood definition, which affects the transition rule in Equation (5), leads to the filling of most of the gaps caused by single trees or shadows, which build one segment. However, there are some missing road segments. This is mostly due to the fact that some rows of trees and their shadows, which hang over narrow roads, divide

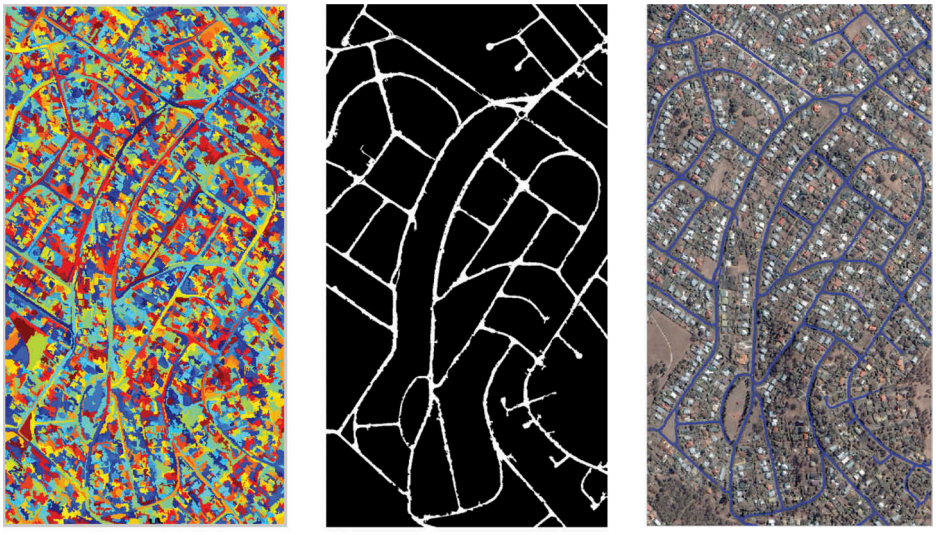

Figure 6. Results of applying the proposed approach on the first study area. (*a*) colour-coded segmentation result; (*b*) ACO-based road detection result; (*c*) final road centrelines superimposed on the image.

them into small segments. Therefore, the ability of the ACO algorithm in leveraging the shape descriptors of the road segments is hampered by the small size of these segments. Some leakages in the segmentation result also increased the incorrect detection, which are strong evidences for the impact of the quality of the segmentation on the final roadmap.

For quantitative evaluation of the result, three metrics mentioned in Section 3.2 are utilized and are listed in Table 1.

As shown in Table 1, the proposed approach yields promising results, with respect to all criteria, which verifies the suitability of the ACO for road extraction from VHR satellite images. Furthermore, the appropriate performance of the proposed approach is because of the well-established object-based heuristics, which are adopted in the ACO algorithm and the effective definition of neighbourhood to suppress the effect of occlusion.

3.5. *Second experiment*

For the second experiment, another test is performed on a challenging part of the Hobart data set, as shown in Figure 7(*a*). Four multispectral bands with 4 m spatial resolution as well as a panchromatic band with 1 m spatial resolution are also used for this experiment. This data set, which covers an area of 1000 × 1000 m, has most of the characteristics of the first data set, such as many dead-ends, different junctions, and

Table 1. Quantitative assessment of the results of the proposed approach.

Completeness (%)	Correctness (%)	Quality (%)
85.6	92.2	79.8

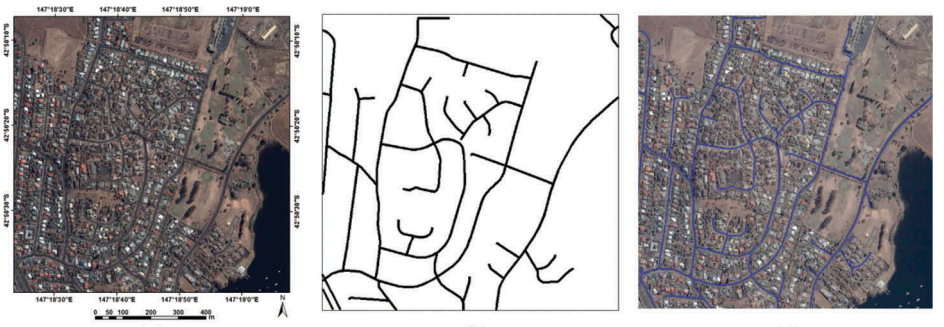

Figure 7. Second study area. (*a*) VHR satellite image of the study area; (*b*) ground truth; (*c*) extraction result.

highly curved roads. Moreover, the existence of an elongated open water area in the right part of the image makes this data set more challenging. There are numerous approaches and indices that can detect water regions in a multispectral image (Xu 2006), but we do not use them to test the performance of our proposed heuristic information in this data set for separating elongated non-road objects.

For this experiment, we use the same parameters as the first experiment, except for roads width range, which is utilized in the heuristic information of the ACO. The maximum and minimum values for roads width in this study area are 18 m and 6 m, respectively

The result of extracting road network of the second data set is shown in Figure 7(*c*). Furthermore, the result of the proposed approach is quantitatively compared with two state-of-the-art methodologies, in Table 2.

Figure 7(*c*) shows that the proposed approach extracted most parts of the road network. Moreover, the open water region is separated efficiently. It is on account of the distance function that is employed in SOLI that is embedded in ACO as the heuristic information.

To assess the relative significance of our approach, a comparison with two state-of-the-art methods is undertaken. These approaches are introduced by Miao et al. in Miao et al. (2015) and Miao et al. (2013), hereafter referred to as 'SVM' and 'MARS', respectively. Both approaches use different object-based descriptors that can show the advantages and limitations of the descriptors introduced in this article as heuristic information of the ACO algorithm. Moreover, the mathematical morphology approach utilized in Miao et al. (2013) and tensor voting and geometric information, which is used in Miao et al. (2015), can be an aptitude test for the modified transition rule of the proposed

Table 2. Quantitative comparison of the results with two state-of-the-art methods.

Method	Completeness (%)	Correctness (%)	Quality (%)
MARS	56	**91**	54
SVM	86	83	73
Proposed Method	**87**	89	**78**

The highest values with respect to the evaluation criteria are given in bold.

ACO method in road gap filling. The quantitative comparison of the results for this data set is listed in Table 2.

As Table 2 indicates, the highest correctness is achieved by the MARS algorithm. Nonetheless, the quality of this approach is strongly attenuated by its low completeness. SVM and our method attain a good balance between completeness and correctness, which leads to superior quality indices. One reason for the better completeness of these approaches is utilizing more discriminating object-based descriptors, which can efficiently distinguish road segments. Moreover, the gap-filling strategies used in SVM and our approach reduce the FNs. It should be emphasized here that, filling the road network gaps only becomes important when a certain level of quality has been reached (Mayer et al. 2006). The completeness of SVM and the proposed method are close to each other. However, the correctness of our approach is better than the SVM method. SVM also needs a training step for each data set, which reduces its automation and transferability. Furthermore, the SVM approach combines tensor voting, active contours, and road geometry information in order to fill the extracted road network gaps. In our approach, continuous ants' movement achieves spontaneous connection of the objects. The main limitation of the proposed approach is that its input data set must contain a band such as a near-infrared band for vegetation discrimination.

According to Mayer et al. (2006), completeness and correctness in a 'practically useful road extraction method' should not be lower than 0.6 and 0.75, respectively. With regard to this definition, SVM and the proposed approach are practically useful approaches. Nevertheless, despite its high correctness, MARS suffers from low completeness of its results in this data set.

4. Conclusion

In this article, a road extraction method based on OBIA and ACO has been presented for the extraction of road network from multispectral VHR satellite images. An innovative desirability function is designed, which enables the ACO algorithm to discriminate the road objects, based on the embedded object-based heuristic information. Furthermore, a new neighbourhood definition in object space is introduced in order to reduce the road gaps. Experiments have demonstrated that the proposed approach can reliably extract roads from multispectral VHR images. It also verifies that our method can handle most gaps, dead-ends, curved roads, and different junction shapes, which are usually problematic situations in road extraction.

The road extraction results obtained by the proposed approach achieved more than 85% for both completeness and correctness criteria. Nonetheless, there are some limitations in our approach. The most important limitation is that the heuristic function in our approach needs a multispectral image containing a band that should be suitable for vegetation discrimination. Most recent commercial Earth observation satellite sensors as well as aerial cameras provide this information. However, we believe that this is a limitation for utilizing useful images from other popular sources of VHR images, which contain just three visible bands, such as Google Maps or Bing maps. In order to address this limitation, we will ameliorate our ACO system, by employing more appropriate descriptors, in our

future research. More improvement can be achieved by utilizing a junction detection strategy and utilizing the extracted junctions as deployment points for the ants.

Acknowledgements

The authors would like to thank the ISPRS and the Space Imaging LLC for providing the IKONOS data set. The authors would also like to thank Professor Timothy Warner and anonymous reviewers for their constructive suggestions, which have enriched this article.

Disclosure statement

No potential conflict of interest was reported by the authors.

ORCID

Mehdi Maboudi http://orcid.org/0000-0003-3367-2404

References

Ameri, F., and M. J. ValadanZoej. 2015. "Road Vectorisation from High-Resolution Imagery Based on Dynamic Clustering Using Particle Swarm Optimisation." *The Photogrammetric Record* 30 (152): 363–386. doi:10.1111/phor.12123.

Baatz, M., and A. Schäpe. 2000. "Multiresolution Segmentation: an Optimization Approach for High Quality Multi-Scale Image Segmentation." In *Angewandte Geographische Informations-Verarbeitung XII*, edited by J. Strobl, T. Blaschke, and G. Griesebner, 12–23. Salzburg, Austria: Wichmann Verlag.

Bennamoun, M., and G. J. Mamic. 2002. *Object Recognition Fundamentals and Case Studies*. London, UK: Springer-Verlag. doi:10.1007/978-1-4471-3722-1_1.

Benz, U. C., P. Hofmann, G. Willhauck, I. Lingenfelder, and M. Heynen. 2004. "Multi-Resolution, Object-Oriented Fuzzy Analysis of Remote Sensing Data for GIS-Ready Information." *ISPRS Journal of Photogrammetry and Remote Sensing* 58 (3–4): 239–258. doi:10.1016/j.isprsjprs.2003.10.002.

Blaschke, T. 2010. "Object Based Image Analysis for Remote Sensing." *ISPRS Journal of Photogrammetry and Remote Sensing* 65 (1): 2–16. doi:10.1016/j.isprsjprs.2009.06.004.

Das, S., T. T. Mirnalinee, and K. Varghese. 2011. "Use of Salient Features for the Design of a Multistage Framework to Extract Roads from High-Resolution Multispectral Satellite Images." *IEEE Transactions on Geoscience and Remote Sensing* 49 (10): 3906–3931. doi:10.1109/TGRS.2011.2136381.

Davoodianidaliki, M., A. Abedini, and M. Shankayi. 2013. "Adaptive Edge Detection Using Adjusted Ant Colony Optimization." In *International Archives of the Photogrammetry, Remote Sensing and Spatial Information Sciences*, edited by H. Arefi, M. A. Sharifi, P. Reinartz, and M. R. Delavar, 123–126. Vol. XL-1/W3. Tehran, Iran: ISPRS. doi:10.5194/isprsarchives-XL-1-W3-123-2013.

Delévacq, A., P. Delisle, M. Gravel, and M. Krajecki. 2013. "Parallel Ant Colony Optimization on Graphics Processing Units." *Journal of Parallel and Distributed Computing* 73 (1): 52–61. doi:10.1016/j.jpdc.2012.01.003.

Dorigo, M., E. Bonabeau, and G. Theraulaz. 2000. "Ant Algorithms and Stigmergy." *Future Generation Computer Systems* 16 (8): 851–871. doi:10.1016/S0167-739X(00)00042-X.

Engelbrecht, A. P. 2007. *Computational Intelligence*. 2nd ed. Chichester, UK: John Wiley & Sons. doi:10.1002/9780470512517.

Floreano, D., and C. Mattiussi. 2008. *Bio-Inspired Artificial Intelligence: Theories, Methods, and Technologies*. Cambridge, MA: The MIT Press.

Grote, A., C. Heipke, and F. Rottensteiner. 2012. "Road Network Extraction in Suburban Areas." *The Photogrammetric Record* 27 (137): 8–28. doi:10.1111/j.1477-9730.2011.00670.x.

ISPRS. 2014. "Data Sets Collection." http://www.isprs.org/data/ikonos_hobart/default.aspx.

Li, M., A. Stein, W. Bijker, and Q. Zhan. 2016. "Region-Based Urban Road Extraction from VHR Satellite Images Using Binary Partition Tree." *International Journal of Applied Earth Observation and Geoinformation* 44 (February): 217–225. doi:10.1016/j.jag.2015.09.005.

Li, Y., L. Xu, and H. Piao. 2009. "Semi-Automatic Road Extraction from High-Resolution Remote Sensing Image: Review and Prospects." In *9th International Conference on Hybrid Intelligent Systems*, edited by J. S. Pan, J. Liu, and A. Abraham, 204–209. Vol. 1. IEEE. doi:10.1109/HIS.2009.317.

Li, Z., W. Shi, Q. Wang, and Z. Miao. 2015. "Extracting Man-Made Objects from High Spatial Resolution Remote Sensing Images via Fast Level Set Evolutions." *IEEE Transactions on Geoscience and Remote Sensing* 53 (2): 883–899. doi:10.1109/TGRS.2014.2330341.

Maboudi, M., and J. Amini. 2015. "Object Based Segmentation Effect on Road Network Extraction from Satellite Images." In *Proceedings of the 36th Asian Conference on Remote Sensing*. Manila, Philippines: ACRS. http://acrs2015.ccgeo.info/proceedings/TH2-3-3.pdf.

Maboudi, M., J. Amini, and M. Hahn. 2016. "Objects Grouping for Segmentation of Roads Network in High Resolution Images of Urban Areas." In *ISPRS - International Archives of the Photogrammetry, Remote Sensing and Spatial Information Sciences*, edited by L. Halounova, F. Sunar, M. Potůčková, L. Patková, M. Yoshimura, U. Sörgel, E. Ben-Dor, et al., 897–902. Vols XLI-B7. ISPRS. doi:10.5194/isprs-archives-XLI-B7-897-2016.

Maboudi, M., J. Amini, M. Hahn, and M. Saati. 2016. "Road Network Extraction from VHR Satellite Images Using Context Aware Object Feature Integration and Tensor Voting." *Remote Sensing* 8 (8): 637. doi:10.3390/rs8080637.

Mahmoudi, T., F. Samadzadegan, and P. Reinartz. 2013. "Object Oriented Image Analysis Based on Multi-Agent Recognition System." *Computers & Geosciences* 54 (April): 219–230. doi:10.1016/j.cageo.2012.12.007.

Mayer, H., S. Hinz, U. Bacher, and E. Baltsavias. 2006. "A Test of Automatic Road Extraction Approaches." In *Symposium of ISPRS Commission III: Photogrammetric Computer Vision (PCV' 06)*, edited by W. Förstner and R. Steffen, 209–214. Bonn, Germany: ISPRS.

Mena, J. B. 2003. "State of the Art on Automatic Road Extraction for GIS Update : A Novel Classification." *Pattern Recognition Letters* 24 (16): 3037–3058. doi:10.1016/S0167-8655(03)00164-8.

Miao, Z., W. Shi, P. Gamba, and Z. Li. 2015. "An Object-Based Method for Road Network Extraction in VHR Satellite Images." *IEEE Journal of Selected Topics in Applied Earth Observations and Remote Sensing* 8 (10): 4853–4862. doi:10.1109/JSTARS.2015.2443552.

Miao, Z., W. Shi, H. Zhang, and X. Wang. 2013. "Road Centerline Extraction from High-Resolution Imagery Based on Shape Features and Multivariate Adaptive Regression Splines." *IEEE Geoscience and Remote Sensing Letters* 10 (3): 583–587. doi:10.1109/LGRS.2012.2214761.

Mirnalinee, T. T., S. Das, and K. Varghese. 2011. "An Integrated Multistage Framework for Automatic Road Extraction from High Resolution Satellite Imagery." *Journal of the Indian Society of Remote Sensing* 39 (1): 1–25. doi:10.1007/s12524-011-0063-9.

Mokhtarzade, M., and M. J. ValadanZoej. 2007. "Road Detection from High-Resolution Satellite Images Using Artificial Neural Networks." *International Journal of Applied Earth Observation and Geoinformation* 9 (1): 32–40. doi:10.1016/j.jag.2006.05.001.

Nikfar, M., M. J. ValadanZoej, M. Mokhtarzade, and M. Shoorehdeli. 2015. "Designing a New Framework Using Type-2 FLS and Cooperative-Competitive Genetic Algorithms for Road Detection from IKONOS Satellite Imagery." *Remote Sensing* 7 (7): 8271–8299. doi:10.3390/rs70708271.

Quackenbush, L. J., J. Im, and Y. Zuo. 2013. "Road Extraction: A Review of Lidar-Focused Studies." In *Remote Sensing of Natural Resources*, edited by W. Guangxing and Q. Weng, 155–170. Remote Sensing Applications Series. Boca Raton, FL: CRC Press. doi:10.1201/b15159-13.

Rahimi, S., H. Arefi, and R. Bahmanyar. 2015. "Automatic Road Extraction Based on Integration of High Resolution Lidar and Aerial Imagery." In *ISPRS - International Archives of the*

Photogrammetry, Remote Sensing and Spatial Information Sciences, edited by H. Arefi and M. Motagh, 583–587. Vol. XL-1-W5. Kish, Iran. doi:10.5194/isprsarchives-XL-1-W5-583-2015.

Ravanbakhsh, M., C. Heipke, and K. Pakzad. 2008. "Road Junction Extraction from High-Resolution Aerial Imagery." *The Photogrammetric Record* 23 (124): 405–423. doi:10.1111/j.1477-9730.2008.00496.x.

Saati, M., J. Amini, and M. Maboudi. 2015. "A Method for Automatic Road Extraction of High Resolution SAR Imagery." *Journal of the Indian Society of Remote Sensing* 43 (4): 697–707. doi:10.1007/s12524-015-0454-4.

Saba, F., M. J. ValadanZoej, and M. Mokhtarzade. 2016. "Optimization of Multiresolution Segmentation for Object-Oriented Road Detection from High-Resolution Images." *Canadian Journal of Remote Sensing* 42 (2): 75–84. doi:10.1080/07038992.2016.1160770.

Saeedi, S., F. Samadzadegan, and N. El-Sheimy. 2009. "Object Extraction from LIDAR Data Using an Artificial Swarm Bee Colony Clustering Algorithm." In *CMRT09. IAPRS, 38(Part 3)*, edited by N. Paparoditis, U. Stilla, and F. Rottensteiner, 133–138. Paris, France: ISPRS.

Samadzadegan, F., and N. Zarrinpanjeh. 2008. "Earthquake Destruction Assessment of Urban Roads Network Using Satellite Imagery and Fuzzy Inference Systems." In *The International Archives of the Photogrammetry, Remote Sensing and Spatial Information Sciences, Vol. XXXVII, Part B8*, edited by J. Chen, J. Jie, and A. Peled, 409–414. Beijing, China: ISPRS.

Schiewe, J. 2002. "Segmentation of High-Resolution Remotely Sensed Data—Concepts, Applications and Problems." In *Symposium on Geospatial Theory, Processing and Applications*, edited by C. Armenakis and Y. C. Lee. Ottawa: ISPRS.

Shi, W., and C. Cheung. 2006. "Performance Evaluation of Line Simplification Algorithms for Vector Generalization." *The Cartographic Journal* 43 (1): 27–44. doi:10.1179/000870406X93490.

Stützle, T., M. López-Ibáñez, P. Pellegrini, M. Maur, M. M. De Oca, M. Birattari, and M. Dorigo. 2012. "Parameter Adaptation in Ant Colony Optimization." In *Autonomous Search*, edited by Y. Hamadi, E. Monfroy, and F. Saubion, 191–215. Berlin, Heidelberg: Springer Berlin Heidelberg.

Wang, M., and R. R. Li. 2014. "Segmentation of High Spatial Resolution Remote Sensing Imagery Based on Hard-Boundary Constraint and Two-Stage Merging." *IEEE Transactions on Geoscience and Remote Sensing* 52 (9): 5712–5725. doi:10.1109/TGRS.2013.2292053.

Wang, W., N. Yang, Y. Zhang, F. Wang, T. Cao, and P. Eklund. 2016. "A Review of Road Extraction from Remote Sensing Images." *Journal of Traffic and Transportation Engineering* 3 (3): 271–282. doi:10.1016/j.jtte.2016.05.005.

Wiedemann, C., C. Heipke, H. Mayer, and O. Jamet. 1998. "Empirical Evaluation of Automatically Extracted Road Axes." In *Empirical Evaluation Techniques in Computer Vision*, edited by K. Bowyer and P. Jonathon Phillips, 172–187. 1st ed. Los Alamitos, CA: IEEE Computer Society Press.

Xu, H. 2006. "Modification of Normalised Difference Water Index (NDWI) to Enhance Open Water Features in Remotely Sensed Imagery." *International Journal of Remote Sensing* 27 (14): 3025–3033. doi:10.1080/01431160600589179.

Yang, X.-S., Z. Cui, R. Xiao, A. H. Gandomi, and M. Karamanoglu. 2013. *Swarm Intelligence and Bio-Inspired Computation: Theory and Applications*. 1st ed. Amsterdam, The Netherlands: Elsevier Science Publishers B. V.

Yin, D., S. Du, S. Wang, and Z. Guo. 2015. "A Direction-Guided Ant Colony Optimization Method for Extraction of Urban Road Information from Very-High-Resolution Images." *IEEE Journal of Selected Topics in Applied Earth Observations and Remote Sensing* 8 (10): 4785–4794. doi:10.1109/JSTARS.2015.2477097.

Zarrinpanjeh, N., F. Samadzadegan, and T. Schenk. 2013. "A New Ant Based Distributed Framework for Urban Road Map Updating from High Resolution Satellite Imagery." *Computers & Geosciences* 54 (April): 337–350. doi:10.1016/j.cageo.2012.12.006.